We are IntechOpen, the world's leading publisher of Open Access books Built by scientists, for scientists

4,800
Open access books available

122,000
International authors and editors

135M
Downloads

Our authors are among the

154
Countries delivered to

TOP 1%
most cited scientists

12.2%
Contributors from top 500 universities

CLARIVATE ANALYTICS BOOK CITATION INDEX INDEXED

WEB OF SCIENCE™

Selection of our books indexed in the Book Citation Index in Web of Science™ Core Collection (BKCI)

Interested in publishing with us?
Contact book.department@intechopen.com

Numbers displayed above are based on latest data collected.
For more information visit www.intechopen.com

1

Hydrodynamics of Dual Fluidized Beds

M.K. Karmakar and P.K. Chatterjee
CSIR-Central Mechanical Engineering Research Institute, Durgapur, West Bengal, India

1. Introduction

A dual fluidized beds system essentially comprises of two fluidized bed reactors coupled together with a provision of gas or materials transfer in between. It may be a combination of circulating-circulating or bubbling-circulating or bubbling-bubbling type systems. A noble application is in a gasification process for coal or biomass where nitrogen of air is not allowed to dilute the product gas. In a dual fluidized bed gasifier of bubbling-circulating type system, a bubbling fluidized bed (BFB) reactor acts as the gasifier where steam is used as gasifying medium to get medium heating value syngas and the circulating fluidized bed is a combustor using air as fluidizing medium. The energy demand for the endothermic gasification reaction is met by the combustion of residual char in the fast bed combustor. The circulating bed materials act as heat carrier between the two fluidized beds and maintain the required temperature in gasifier. Therefore, the hydrodynamics of such a dual fluidized beds system needs to be thoroughly understood for successful design and operation of the system for industrial application.

In literature, the studies on hydrodynamics of bubbling fluidized bed and circulating fluidized bed systems are available separately. However, the studies on hydrodynamics of combined system of these, a dual fluidized beds system loop predictions are scanty. The flow structure of gas-solids mixture is very complex in CFB system. Variety of models of fluidized bed system have been classified into three broad groups: (i) models predicting solids suspension density in axial variation, but not in radial direction, (ii) models predicting axial and radial variations by assuming two or more regions, such as core-annulus or clustering annulus flow models and (iii) models which employ the fundamental equations of fluid dynamics to predict the two phase gas-solids flow (Harris & Davidson, 1994). Of the three classifications, the type (iii) seems to be most rigorous, but the mathematical complexity of solving the equations limits its usefulness from practical design perspective. According to literature (Pugsley & Berruti, 1996a, 1996b), it is suggested that type (i) and type (ii) models are the best suited as a design tool for CFB to investigate the effects of operating conditions and riser dimensions on the flow structure. A dual fluidized beds system was also investigated (Bai et al., 1997) with two risers, two downcomers and two valves. The model shows how the solids circulation fluxes are affected by the operating conditions such as superficial gas velocities, particle diameter, density, solids inventory and fractional opening of solids flow control valves as well as by geometry. The hydrodynamics of a dual fluidized beds system were also studied (Loffler et al. 2003; Kaiser et al., 2003) which consisted of a fast bed riser with the downcomer, a

bubbling bed gasifier and a transfer pipe. They used the loop seals arrangement for solids flow control in the system.

2. Description

In this section, the hydrodynamics of a dual fluidized beds has been discussed using the almost similar system as described in (Loffler et al. 2003; Kaiser et al., 2003) except the mechanism for the solids transfer between the vessels. Loop seal device has been used in the studies described in (Loffler et al. 2003; Kaiser et al., 2003). In the current study, two L-valves, in place of loop seals, have been installed between the coupled reactors. The L-valves absorb a part of pressure that is built up due to static head of solids in the downcomer. Depending upon the pressure absorbed in L-valves, the solid circulation rate changes to adjust the pressure balance of the loop.

2.1 Experimental test set up

The dual fluidized beds experimental set up is made of transparent perspex material. The system consists of a fast bed riser, a cyclone to separate the solids, a down comer with a L-valve, a bubbling fluidized bed and a return pipe with another L-valve. The system is shown schematically in Fig 1. The solids after passing through the fast bed riser gets separated in the cyclone, descend downwards through the down comer and enter the bubbling bed reactor through the L-valve. A part of bed materials in the bubbling bed system are then transferred back into the riser through the inclined return leg fitted with the other L-valve. Circulation of material takes place in this way. The major dimensions of test set-up and the range of operating flow rates are presented in Table 1.

Parameter	Value	Unit
Height of riser	5.95	m
Inside diameter of riser	0.050	m
Height of Secondary air injection above distributor	0.300	m
Height of bubbling fluidized bed vessel	1.200	m
Inside diameter of bubbling fluidized bed vessel	0.100	m
Length of downcomer stand pipe	4.0	m
Inside diameter of downcomer stand pipe	0.025	m
Connecting pipe diameter: fast bed and bubbling bed	0.025	m
Primary air flow in fast bed riser	1.5 – 5.0	m^3/hr
Secondary air flow in fast bed riser	25-50	m^3/hr
Air flow in bubbling fluidized bed vessel	3-16	m^3/hr

Table 1. Dimensions and air flow rates of dual FB system cold model set up

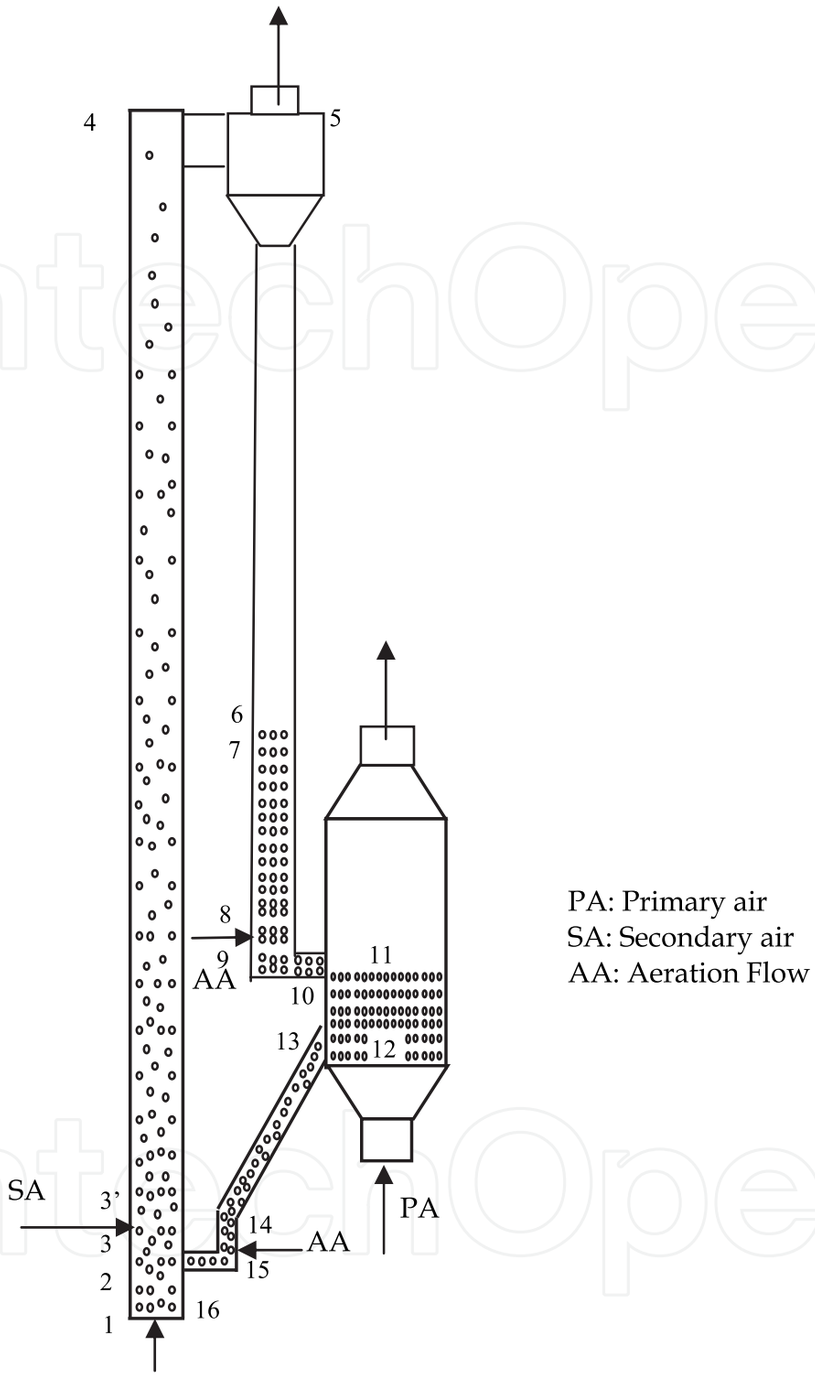

Fig. 1. Schematic diagram of dual FB system: 1-2: Dense zone, 2-3: Splash zone, 3-3′: Secondary air injection, 3′-4: Transport zone, 4-5: Cyclone separator, 5-6: Downcomer above sand accumulation column, 6-7: Air Sand Interface 7-8: Sand accumulation in downcomer, 8-9: Aeration point, 9-10: Aeration point to solid discharge point, 10-11: Solid discharge to bubbling bed, 11-12: bubbling fluidized bed gasifier, 12-13: Connector junction, 13-14: Connector from bubbling to Aeration point, 14-15: Aeration point, 15-16: Aeration point to solid discharge to fast bed

The description of the cold model set up is discussed below.

Fast bed riser: The system consists of a 5.95 m high and 0.05 m inner diameter riser made of transparent perspex. It is fitted with a perforated type distributor plate at the bottom. There are two air flow systems in riser. The primary air is given through the distributor plate where the flow is controlled by a regulator valve for maintaining the bottom bed at bubbling fluidizing state. The secondary air is injected in fast bed riser above the connector point from the bubbling bed vessel at a height of 0.3 m above the distributor plate. The size of secondary air port is 0.025 m in the riser. The secondary air helps to pneumatically transport the sand particles to the top of riser before entering into the cyclone separator. The flow rates of primary and secondary air in riser and the fluidizing air to bubbling bed vessel were measured by the orifice meters.

Cyclone: The cyclone separates the silica sands from the gas-solid mixture and feeds the solid material to the down comer. The entry duct to cyclone is placed tangentially with the cyclone body so that the gas-solids mixture experiences a rotational movement forming a vortex inside the cyclone causing the heavier particles to fall down. The air leaves through the upward escape pipe. The outside diameter of cyclone is 0.1 m while the delivery pipe is 0.05 m in diameter. The figure of the cyclone is shown in Fig 2.

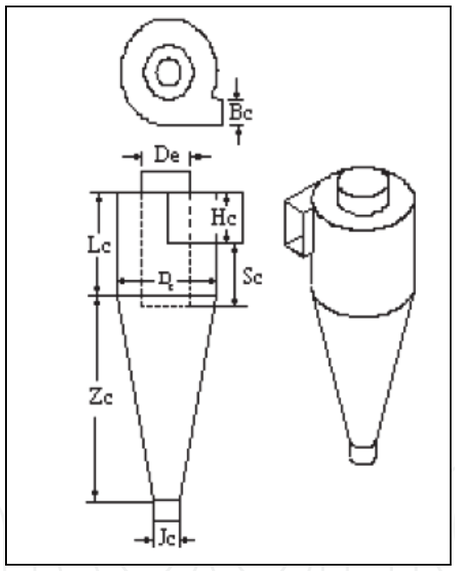

Bc = 25 mm
Hc = 50 mm
Dc = 100 mm
De = 50 mm
Lc = 200 mm
Zc = 300 mm
Jc = 25 mm

Fig. 2. Cyclone dimensions in dual FB system

Downcomer and L-valve: The down comer is a transparent perspex pipe of inner diameter of 0.025 m. The height of downcomer pipe is 4.0 m. There is a L-valve at the bottom of downcomer pipe. The L-valve is meant for controlling the solid sand flow to the gasifier by means of air flow regulation. The port size of L-valve is 0.006 m for air injection. The length of horizontal leg of L-valve is 0.1 m which extends upto the bubbling bed vessel.

Bubbling bed system: The bubbling fluidized bed is also made of perspex pipe of inside diameter 0.1 m and of 1.2 m high. There is a distributor plate at the bottom of the gasifier. The distributor plate is a single perforated plate. There is an opening for under-bed feeding of fresh sand inside the vessel. The primary air flow from a blower keeps the bed in bubbling condition.

Connector and L-valve: The connector is an inclined transparent pipe of inner diameter of 0.03 m. The vertical height is 1.3 m with a L-valve arrangement. The solids sand materials in the bubbling bed chamber are transferred to the fast bed riser through the aeration flow regulated by L-valve. The port size in the L-valve is 0.006 m for auxiliary air injection. The length of horizontal leg of L-valve is 0.1 m through which the fast bed riser is connected to complete the loop.

Feeding system of bed materials: The bed material feeding system consists of a screw feeder and a lock hopper, the screw feeder is connected to a variable speed motor. The screw feeder feeds the solid bed materials directly into the bubbling bed at the height of 0.1 m above the distributor. The sand particles ranging from 0.147 mm to 0.416 mm in mean diameters have been used as bed materials. The hopper is refilled manually with bed materials periodically.

There are eight numbers of pressure taps along the riser height to measure the static heads. Similarly, there is one pressure tap at cyclone, five in downcomer and L-valve section, two in bubbling fluidized bed and three in the connection pipe. The pressure heads have been measured using water manometers. A blower has been used to supply air to the system.

2.2 Materials and method

To investigate the hydrodynamic behaviour, four silica sand samples (group-B particles as per Geldart classification) of different Sauter mean diameters have been taken during the experiments. These samples are prepared by screening the materials through a set of wire mesh sieves. The characteristics of bed material are presented in Table 2. The cumulative percentage distribution for each mean particle size is shown in Fig 3.

Material	Sand I	Sand II	Sand III	Sand IV
Size range, μm	50-300	75-425	106-500	150-600
Mean diameter, μm	147	211	334	416
Sphericity	0.86	0.86	0.86	0.86
Particle density, kg/m^3	2650	2650	2650	2650
Bulk density, kg/m^3	1696	1696	1710	1722
Voidage at min. fluidization, ε_{mf}	0.46	0.44	0.41	0.40
Min fluidization velocity at 27 ^{0}C, m/s	0.018	0.037	0.091	0.138
Particle terminal velocity at 27 ^{0}C, m/s	1.2	1.7	2.7	3.4
Archimedes' number	281	835	3292	6347
Group of Geldart's classification	B	B	B	B

Table 2. Characteristics of the bed materials used during cold model analysis

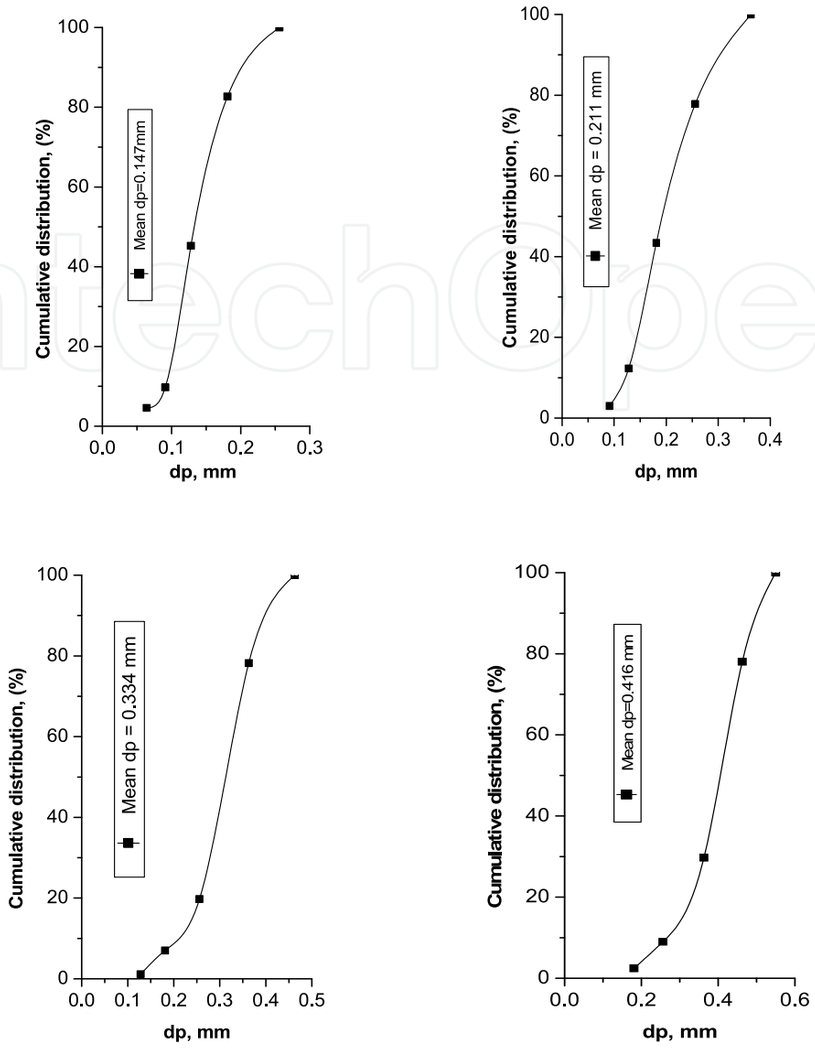

Fig. 3. Cumulative particle size distribution of silica sand samples

Separate aeration flows have been used through two L-valves to maintain the material circulation in the dual bed system. The aeration taps are placed near the valve bend in downcomer which yields the maximum solids flow. The solids do not begin to flow immediately upon injecting aeration flow; there is a threshold aeration rate to produce a drag force sufficient to initiate solids flow. When this drag force exceeds the force required to overcome the resistance to solids moving through the constricting bend and gravity of the particles, the solids begin moving through this non-mechanical valve (Knowlton, 1997).

Each run was characterized at a fixed primary air flow with variations in secondary air and aeration flow. The solids inventory in all runs was maintained at 6.0 kg. The solid circulation rate is an essential parameter in a dual fluidized bed system and hence, its measurement is an important experimental input. It may be measured through a very simple way. In this study, when the gas-solids flow was fully established in the system, the flow of material in downcomer was suddenly stopped by closing the L-valve for a short duration. The increase in height of materials, piled up in downcomer, was measured to determine the solid circulation.

Under steady state conditions during experiment, the solids circulation rate, primary and secondary air in riser and the readings at static pressure points are noted. By varying the riser air velocity and aeration flow, the solids circulation rate and the system pressure at different points are taken at different operating conditions.

2.3 Modeling

2.3.1 Riser

The axial pressure profile in riser is a key parameter and an important characteristic of CFB; the prediction of such profile is a major task in modeling the system. The pressure drop in riser is usually contributed by the pressure heads for solids suspension, gas solids friction and particle acceleration.

The current model assumes the CFB riser to be divided into three regions: dense bottom zone, splash zone and dilute transport zone. When the gas passes through the bottom zone, a distinct bed surface separates the bed which enables some particles of solids to entrain into the splash zone. A part of these entrained particles becomes decelerated and return back to the bottom zone, while the rest of the particles are accelerated to the transport zone. It is most likely that acceleration on a time average is compensated for by the corresponding deceleration. The only net acceleration is that caused by the secondary air, and it is small in the present case. Secondary air helps in the process of solids transportation and the axial voidage is the major factor for determining the solids circulation in the system.

Dense zone: The dense bottom bed operates in bubbling fluidized mode and it comprises of two phases, namely, a dense or emulsion phase and a bubble phase. The volume fraction of solids in such bed is obtained by applying modified two phase theory (Johnsson et al., 1991). The emulsion phase is formed by the bed particles as well as the interstitial gas flow in bed particles. The gas velocity, U_{mf}, and the voidage, ε_{mf}, at minimum fluidizing condition is determined from literature (Ergun, 1952).

$$U_{mf} = \frac{\mu_g}{d_p \rho_g}\left[\left(33.7^2 + 0.0408\frac{d_p^3 \rho_g \left(\rho_s - \rho_g\right) g}{{\mu_g}^2}\right)^{\frac{1}{2}} - 33.7\right] \tag{1}$$

and

$$\frac{\Delta p}{L_{mf}} = \left(1 - \varepsilon_{mf}\right)\left(\rho_s - \rho_g\right)\frac{g}{g_c} \tag{2}$$

The bubble phase consists of up rising gas bubbles, assumed to be free of solids. The net voidage in the dense zone, ε_{dz}, is expressed as follows.

$$\varepsilon_{dz} = \delta_b + (1 - \delta_b).\varepsilon_{mf} \tag{3}$$

where, the bubble volume fraction, δ_b, can be calculated as:

$$\delta_b = \frac{1}{1 + \frac{1.3\,(\,0.15 + U_{pa} - U_{mf}\,)^{0.33}}{0.26 + 0.7\exp\,(\,-3.3\,d_p\,)}.(\,U_{pa} - U_{mf}\,)^{-0.8}} \tag{4}$$

The bottom zone is characterized by a constant pressure drop for a particular bed height. This constant pressure drop, ΔP_{dz}, is determined by static heads of bed particles with the assumption that solids acceleration and deceleration compensates each other as well as negligible friction forces exist amongst solid bed particles and particles to wall. Therefore, it is given as follows:

$$\Delta P_{dz} = (1 - \varepsilon_{dz})\,\rho_s\,h_{dz}\,g \tag{5}$$

where, h_{dz} is the bed height in dense bubbling zone.

Splash zone: The splash zone is assumed to exist when the gas velocity is below the terminal velocity, U_t, of a single particle above the dense zone. The bubbles erupt ejecting solids above dense bed, some of which fall back again into the bed. This zone extends to secondary air injection level, above which the gas velocity exceeds the terminal velocity. The bed voidage in splash zone, ε_{sz}, is calculated using the following correlation (Kaiser et al., 2003).

$$\frac{\varepsilon_{sz} - \varepsilon}{\varepsilon_{dz} - \varepsilon} = \exp[\,-k(h_{sz} - h_{dz})\,] \tag{6}$$

Since this zone has been considered up to secondary air injection point and the gas velocity in the splash zone is below the single particle terminal velocity, the value of ε has been taken as unity (Loffler et al. 2003). Since this splash zone originates from the upper surface of dense bed, the actual bed height may be taken as (h_{sz} – h_{dz}). The decay factor, k, for the zone has been taken (Johnsson & Leckner, 1995) as

$$k = \frac{C\,U_t}{U_{pa}} \tag{7}$$

where, C = 10 m^{-1}.

For pressure drop estimation in splash zone, one has to consider the local solids hold up. However, there is experimental evidence that the solids acceleration significantly affects the pressure drop across the splash zone (Schlichthaerle & Werther, 1999). Further work is still needed on this issue. The following equation gives the pressure drop in splash zone for solids hold up (Loffler et al. 2003).

$$\Delta P_{sz} = \int_{h_{dz}}^{h_{sz}} (1 - \varepsilon_{sz})\,\rho_s\,g\,dh \tag{8}$$

Now, the ε_{SZ} in eqn. (8) can be represented by ε(h) as a function of height in the splash zone and the equation may be rewritten as

$$\Delta P_{sz} = \int_{h_{dz}}^{h_{sz}} (1 - \varepsilon(h))\,\rho_s\,g\,dh \tag{9}$$

Substituting the value of ε_{sz} from eqn. (6) as unity (Loffler et al. 2003), one gets

$$\Delta P_{sz} = \int_{h_{dz}}^{h_{sz}} \left(1 - \left(1 - (1 - \varepsilon_{dz}) \cdot e^{-k(h - h_{dz})}\right)\right) \rho_s \, g \, dh \tag{10}$$

$$\Rightarrow \Delta P_{sz} = \int_{h_{dz}}^{h_{sz}} \left((1 - \varepsilon_{dz}) \cdot e^{-k(h - h_{dz})}\right) \rho_s \, g \, dh \tag{11}$$

$$\Rightarrow \Delta P_{sz} = (1 - \varepsilon_{dz}).\rho_s.g.e^{k.h_{dz}} \int_{h_{dz}}^{h_{sz}} e^{-k.h} dh \tag{12}$$

$$\Rightarrow \Delta P_{sz} = \left(\frac{(1 - \varepsilon_{dz}).\rho_s.g.e^{k.h_{dz}}}{-k}\right)\left[e^{-k.h_{sz}} - e^{-k.h_{dz}}\right] \tag{13}$$

$$\Rightarrow \Delta P_{sz} = \left(\frac{(1 - \varepsilon_{dz}).\rho_s.g.e^{k.h_{dz}}}{k}\right)\left[\frac{1}{e^{k.h_{dz}}} - \frac{1}{e^{k.h_{sz}}}\right] \tag{14}$$

Transport zone: The axial distribution of voidage profile in transport zone may be obtained from the exponential correlation based on entrainment model (Zenz & Weil, 1958).

$$\frac{\varepsilon_{tz} - \varepsilon_{\infty}}{\varepsilon_{sz} - \varepsilon_{\infty}} = \exp\left[-a\,(h_{tz} - h_{sz})\right] \tag{15}$$

where α is the decay factor of solids fraction and h_{tz} is the height of any point in transport zone.

Various correlations for the decay factor, α, are available in the literature. The present study is dimensionally almost similar to an experiment (Adanez et al., 1994) conducted in a circulating fluidized bed system. They used sand and coal as bed materials under group B of Geldart classification and proposed a correlation for the decay factor.

$$a(U - U_t)^2 \, D^{0.6} = 0.88 - 420\, d_p \tag{16}$$

This correlation has been chosen for the present study as the current operating conditions fall within the range described in literature (Adanez et al., 1994).

The far upstream voidage in transport section, ε_{∞}, in eqn. (15), depends on superficial gas velocity, particle terminal velocity, particle density and elutriation rate. The voidage at infinity is taken as described in (Loffler et al., 2003).

$$(1 - \varepsilon_{\infty}) = \frac{K_{\infty}}{\rho_S\,(U - U_t)} \tag{17}$$

where, K_{∞} is the particle elutriation rate constant for mono-sized bed materials and it is obtained using following correlation (Wen & Chen, 1982).

$$K_{\infty} = \rho_S \, \alpha_i \, (U - U_t) \tag{18}$$

where,

$$\alpha_i = 1 - \left(1 + \frac{f_s \, (U - U_t)^2}{2 \, g \, D}\right)^{-\frac{1}{4.7}} \tag{19}$$

Here, the co-efficient of friction, f_s, is evaluated from the correlations (Wen & Chen, 1982).

$$\frac{f_s \, \rho_S}{d_p^2}\left(\frac{\mu_g}{\rho_g}\right)^{2.5} = 5.17 \left[\frac{\rho_g \, (U - U_t) \, d_p}{\mu_g}\right]^{-1.5} D^2 \quad for \quad \frac{\rho_g \, (U - U_t) \, d_p}{\mu_g} \leq \frac{2.38}{D} \tag{20}$$

and

$$\frac{f_s \, \rho_S}{d_p^2}\left(\frac{\mu_g}{\rho_g}\right)^{2.5} = 12.3 \left[\frac{\rho_g \, (U - U_t) \, d_p}{\mu_g}\right]^{-2.5} D \quad for \quad \frac{\rho_g \, (U - U_t) \, d_p}{\mu_g} \geq \frac{2.38}{D} \tag{21}$$

The eqns. (18) to (21) were recommended for bed particles having diameters in the range of 37 to 3400 μm and density of 860 to 7850 kg/m^3 with superficial velocity in the range of 0.1 to10 m/s in riser with diameters in the range of 0.034 to 2.06 m (Wen & Chen, 1982). The input parameters of present investigation fall within the range as mentioned (Wen & Chen, 1982) and thus, the similar correlations have been used.

The pressure drop in transport zone of riser is determined from the solids hold up which can be represented by the following formulations.

$$\Delta P_{tz} = \int_{h_{sz}}^{h_{tz}} (1 - \varepsilon_{h_{tz}}) \, \rho_s \, g \, dh \tag{22}$$

$$\Rightarrow \Delta P_{tz} = \int_{h_{sz}}^{h_{tz}} \left(1 - \varepsilon(h)\right) \rho_s \, g \, dh \tag{23}$$

$$\Rightarrow \Delta P_{tz} = \int_{h_{sz}}^{h_{tz}} \left[1 - \left(\varepsilon_{\infty} - (\varepsilon_{\infty} - \varepsilon_{sz}) \, . \, e^{-a\left(h - h_{sz}\right)}\right)\right] \rho_s \, g \, dh \tag{24}$$

$$\Rightarrow \Delta P_{tz} = \int_{h_{sz}}^{h_{tz}} \left[\left(1 - \varepsilon_{\infty}\right) + (\varepsilon_{\infty} - \varepsilon_{sz}) \, . \, e^{-a\left(h - h_{sz}\right)}\right] \rho_s \, g \, dh \tag{25}$$

$$\Rightarrow \Delta P_{tz} = \int_{h_{sz}}^{h_{tz}} \left[\left(1-\varepsilon_{\infty}\right) \rho_s \, g \right] dh + \int_{h_{sz}}^{h_{tz}} \left[\left(\varepsilon_{\infty} - \varepsilon_{sz}\right) . e^{-a\left(h - h_{sz}\right)} \right] \rho_s \, g \, dh \tag{26}$$

$$\Rightarrow \Delta P_{tz} = \left(1-\varepsilon_{\infty}\right) \rho_s \, g \left(h_{tz} - h_{sz}\right) + \left(\varepsilon_{\infty} - \varepsilon_{sz}\right) . \rho_s . g . e^{a h_{sz}} . \int_{h_{sz}}^{h_{tz}} \left[e^{-ah} \right] dh \tag{27}$$

$$\Rightarrow \Delta P_{tz} = \left(1-\varepsilon_{\infty}\right) \rho_s \, g \left(h_{tz} - h_{sz}\right) + \left(\frac{\left(\varepsilon_{\infty} - \varepsilon_{sz}\right) . \rho_s . g . e^{a.h_{sz}}}{a} \right) \left[\frac{1}{e^{a.h_{sz}}} - \frac{1}{e^{a.h_{tz}}} \right] \tag{28}$$

The pressure drop due to solids friction is obtained (Loffler et al., 2003) as follows:

$$\Delta P_{tz,fric} = \int_{h_{sz}}^{h_{tz}} f_s \frac{U_S^2}{2} \frac{4}{D} \left(1 - \varepsilon_{h_{tz}}\right) \rho_s \, g \, dh \tag{29}$$

Since the transport section in riser appears to behave like a fully developed dilute-phase vertical pneumatic zone, the correlation for estimating particle velocity beyond the acceleration region (Yang, 1978) has been employed.

$$U_s = U - U_t \sqrt{\left(1 + \frac{f_s U_s^2}{2 g D} \right)} \, \varepsilon_{tz}^{4.7} \tag{30}$$

where,

$$f_s \frac{\varepsilon_{tz}^{\ 3}}{\left(1-\varepsilon_{tz}\right)} = 0.0126 \left[\left(1-\varepsilon_{tz}\right) \frac{U_t}{U_s} \right]^{-0.979}, \quad for \quad \frac{U_t}{U_s} > 1.5 \tag{31}$$

and

$$f_s \frac{\varepsilon_{tz}^{\ 3}}{\left(1-\varepsilon_{tz}\right)} = 0.0410 \left[\left(1-\varepsilon_{tz}\right) \frac{U_t}{U_s} \right]^{-1.021}, \quad for \quad \frac{U_t}{U_s} < 1.5 \tag{32}$$

The equations (15) to (32) are solved iteratively to evaluate the voidage ε_{tz}, the solid friction factor, f_s, and the solid velocity, U_s.

The solids circulation rate, G_s, has been determined from the following correlation:

$$G_s = \rho_s \left(1 - \varepsilon_{tz}\right) U_s \tag{33}$$

2.3.2 Riser exit and cyclone

Riser exit: The pressure drop in horizontal section between riser and cyclone has been considered as available in literature (Patience et al., 1990).

$$\Delta P_{RE} = G_s \left(2.84 + 0.0108\, U_h^2 \right) \tag{34}$$

where, G_s and U_h are the solid mass flux and the gas velocity in this section respectively.

Cyclone: The cyclone pressure drop is directly proportional to the square of inlet velocity and it is employed (Gimbun et al., 2005).

$$\Delta P_{CYC} = \alpha \, \frac{\rho_g U_{CYC}^2}{2} \tag{35}$$

where, α is a function of cyclone dimension and it is expressed in (Gimbun et al., 2005) as.

$$\alpha = 16 \, \frac{a_{CYC} . b_{CYC}}{D_e^2} \tag{36}$$

2.3.3 Down comer and L-valve

The determination of gas flow rate and the corresponding pressure drop through the down comer and L-valve sections of a circulating fluidized bed system is not an easy task (Daous & AI-Zahrani, 1998).

Variations of voidage in downcomer depend on solids flow mode. Non-fluidized bed flow is divided into a packed bed and transitional packed bed flow. In present study, the solids movement in downcomer was considered to be transitional packed bed flow in presence of aeration flow through L-valves. When these aeration taps are turned off, the solids form a packed bed in the downcomer causing no solids flow. While the aeration flow is on, air flows through the particles and the relative movement between gas and solids produces a drag force on the particles in the direction of flow. This phenomenon was also observed in literature (Zhang & Rudolph, 1991) that the transitional packed bed flow occurs when the solids flow by aeration.

During the transitional packed bed flow, the voidage increases linearly with slip velocity. The voidage in downcomer is more than compact bed voidage (ε_c), but less than voidage at minimum fluidization condition (ε_{mf}). Therefore, this voidage above the aeration point is taken as per the correlation (Tong et al., 2003).

$$\varepsilon_{DC} = \frac{1}{2} \left(\varepsilon_{mf} + \varepsilon_c \right) \tag{37}$$

Pressure drop due to solids flow by aeration is a function of slip-velocity as suggested in (Ergun, 1952; Knowlton & Hirsan, 1978).

$$\frac{\Delta P_{DC}}{L_{DC}} = \frac{150\, \mu \, (1-\varepsilon_{DC})^2 \, U_{SLDC}}{(\phi \, d_p)^2 \, \varepsilon_{DC}^2} + \frac{1.75\, \mu \, (1-\varepsilon_{DC}) \, U_{SLDC}^2}{(\phi \, d_p) \, \varepsilon_{DC}} \tag{38}$$

The slip velocity for gas flowing up the downcomer can be expressed as:

$$U_{SLDC} = \frac{G_S}{\rho_S\,(1-\varepsilon_{DC})} + \frac{U_{GDC}}{\varepsilon_{DC}} \tag{39}$$

The slip velocity for gas flowing down the downcomer can be expressed as:

$$U_{SLDC} = \frac{G_S}{\rho_S\,(1-\varepsilon_{DC})} - \frac{U_{GDC}}{\varepsilon_{DC}} \tag{40}$$

For the pressure drop across the L-valve section, ΔP_{LV}, between the aeration point and the solids discharge point to the gasifier can be correlated with the solid mass flux (G_S), L-valve diameter (D_{LV}), mean particle size (d_p) and length of valve (L_{LV}). This correlation is as follows (Geldart & Jones, 1991).

$$\frac{\Delta P_{LV}}{L_{LV}} = 216\, G_S^{\,0.17}\, D_{LV}^{-0.63}\, d_p^{-0.15} \tag{41}$$

This correlation has been used in the present study because the input operating parameters match with those of (Geldart & Jones, 1991). They carried out measurements of valve pressure drops between the aeration and the solids discharge taking silica sand materials with diameters 68-341 μm with density 2550 kg/m^3 and showed that the values estimated by eqn. (41) were close enough with the experimental data.

2.3.4 Bubbling fluidized bed system

The gasifier is considered as bubbling fluidized bed, thus the correlations for pressure drop and voidage are the same as described in article 2.3.1 for dense zone of the riser.

2.3.5 Connector between bubbling and fast bed

The main task of the connector is to prevent the gas slip between the gasifier and the combustor, and excess aeration at L-valve must be avoided to prevent the dilution of product gas in gasifier. The solids circulation from bubbling fluidized bed to fast bed riser is done by an inclined connector pipe with a L-valve. The determination of gas flow rate and the corresponding pressure drop through this inclined connector and L-valve sections of a dual fluidized beds system is done in line with article 2.3.3 (Knowlton & Hirsan, 1978). In this case, the angle of inclination has been taken into account while calculating the pressure drop.

The pressure drop in L-valve has been determined in the same way as described in article 2.3.3.

2.4 Experimental observation

This part describes the experimental investigations which were carried out on hydrodynamics of dual fluidized beds system. The study focused on the axial voidage, the pressure drops across various components and the solid circulation under different

operating conditions. A mathematical model of the system to study its hydrodynamic behavior has been presented. The experimental data have been compared with the mathematical model as discussed in article 2.3.

2.4.1 Voidage profile

The effect of bed particles of mean diameters 0.147 mm and 0.416 mm on voidage along the riser has been predicted as shown in Fig 4, where the primary air flows were maintained at 0.16 m/s and 0.59 m/s respectively at the bottom zone to maintain the bed in fluidized state. It is evident from part A of Fig 4 that the voidage at the dense zone is more for smaller particles compared to larger particles at low air velocity. This can be explained by the fact that both the large and fine particles are present at the bottom zone and fine particles are embedded in larger diameter particles which decreases the voidage.

Due to the secondary air injection, the voidage in the acceleration zone of riser increases to the level of 0.998 as shown in part B of Fig 4. Beyond this acceleration zone, the flow is fully developed and behaves like a dilute-phase vertical pneumatic transport system. It is seen in part C of Fig 4 that, for the superficial gas velocities of 4.43–4.45 m/s, the voidage is more in case of 0.416 mm diameter particle as compared to 0.147 mm diameter particles. This results in lower mass flux for larger particles.

Fig 5 shows the axial voidage of dual fluidized beds system using sand # II. The system has two major sub-systems, (a) the fast bed section – riser, and (b) the section comprising of downcomer, L-valve to bubbling bed, the bubbling bed and the connector to fast bed riser. The voidage along the riser has been indicated from point-1 to point-4 and the voidage in downcomer, L-valve to bubbling bed, the bubbling bed, connector and the L-valve to fast bed riser is shown from point-7 to point-16.

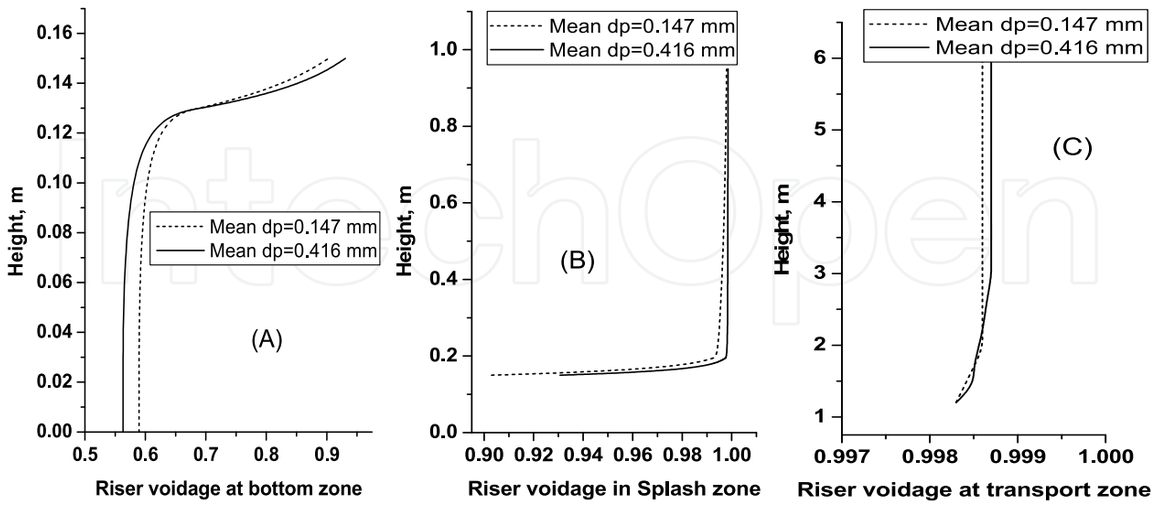

Fig. 4. Riser voidage for sand # I and sand # IV A) at bottom zone (Primary air velocity: 0.16 m/s for sand # I and 0.59 m/s for sand # IV), B) at secondary air injection in splash zone, and C) at transport zone (superficial velocity of 4.43-4.45 m/s)

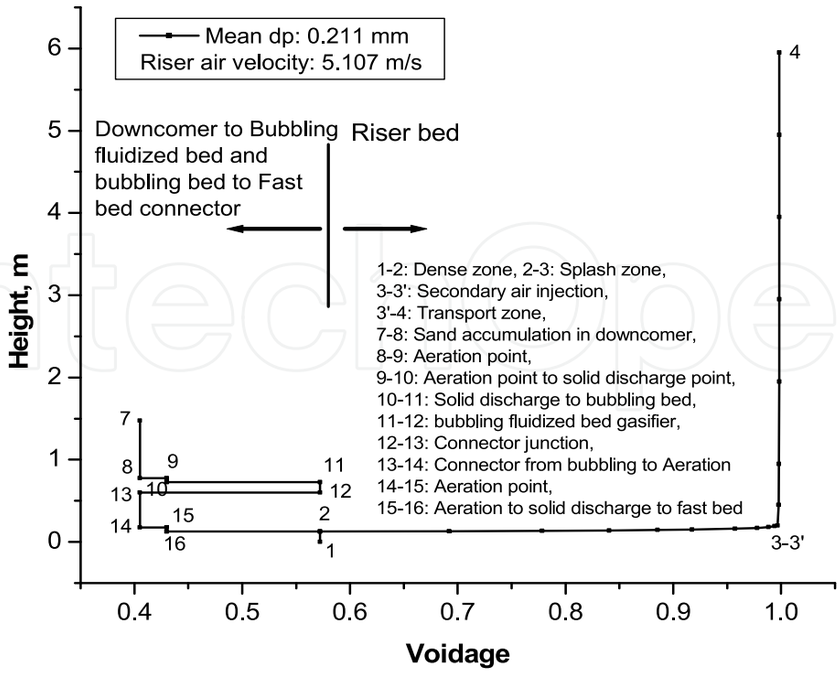

Fig. 5. Axial voidage in Dual Fluidized Bed system for sand # II

2.4.2 Pressure profile

The basic assumption is that the hydrostatic head of solids contributes to the axial pressure drop. The suspension density is related to the pressure drop through the axial distance. During the experiment, the static heads were measured along the riser, at the cyclone, along the downcomer and L-valve, the bubbling fluid bed, the connector and L-valve for every run. It was observed that the pressure drops in components of the loop were affected due to changes in superficial air velocity or solid mass flux.

Fig 6 shows the predicted and experimental values of static pressure for sand # II particles at superficial air velocity 3.85 m/s with solid mass flux of 6.94 kg/m^2-s. The figure indicates that the highest pressure is at downcomer L-valve aeration tap in the loop.

In Fig 7, the static pressure profiles using sand # IV particles have been shown along the dual fluidized beds loop at different rates of mass flux. The figure shows that the pressure drop in L-valve is greater at higher mass flux due to higher aeration flow. This is due to increase in the contribution of drag and weight forces caused by solids flow. This behaviour agrees with (Arena et al. 1978). It is also studied (Kim et al., 1999) that, at constant solids inventory, the pressure drop across the down comer increases with increasing solid circulation rate.

According to literature (Knowlton & Hirsan, 1978), the L-valve pressure drop does not depend on the particle diameter, but, later on, it was reported that the pressure drops in L-valve are less for larger particle diameters (Arena et al. 1978). They attributed this behaviour to the fact that coarser particles produce larger inter particle voidage, thus reducing the resistance to the gas flow. In Fig 8, it is seen that, in the same range of G_s, the L-valve pressure drop was more when smaller particles were used. However, further investigation should be conducted in order to confirm the results.

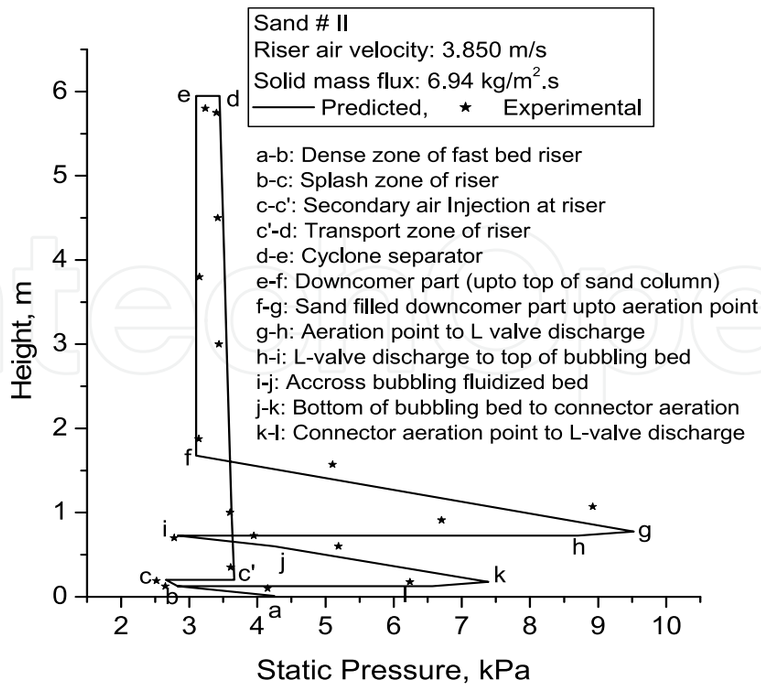

Fig. 6. Predicted and experimental pressure profiles of dual fluidized bed for sand # II

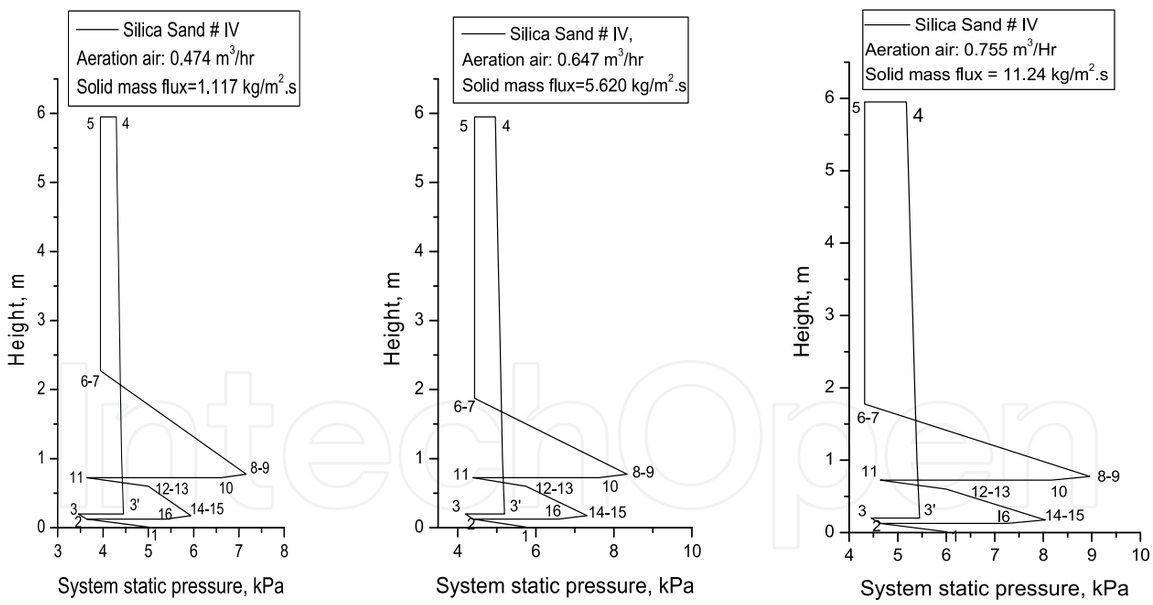

Note: 1-2: Dense zone, 2-3: Splash zone, 3-3': Secondary air injection, 3'-4: Transport zone, 4-5: Cyclone separator, 5-6: Downcomer above sand accumulation column, 6-7: Air Sand Interface 7-8: Sand accumulation in downcomer, 8-9: Aeration point, 9-10: Aeration point to solid discharge point, 10-11: Solid discharge to bubbling bed, 11-12: bubbling fluidized bed gasifier, 12-13: Connector junction, 13-14: Connector from bubbling to Aeration point, 14-15: Aeration point, 15-16: Aeration point to solid discharge to fast bed

Fig. 7. Predicted pressure profiles of dual fluidized bed for sand # IV at different riser air velocities

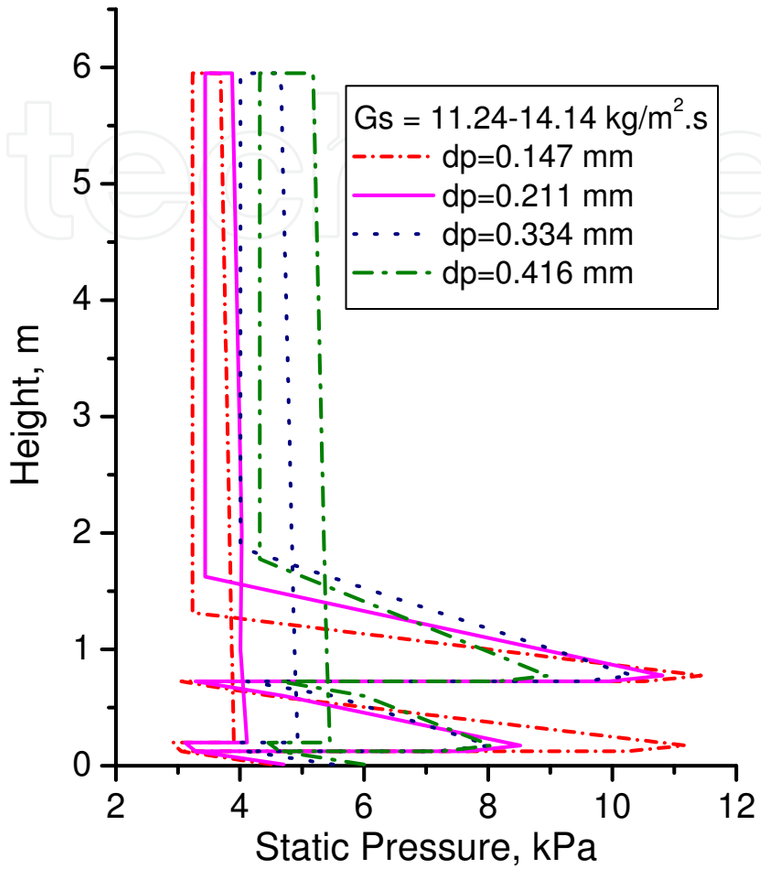

Fig. 8. Predicted pressure profiles in dual fluidized bed for sand # I, II, III and IV

2.4.3 Solid circulation

Fig 9 shows the variations of solid mass flux with the change in aeration flow and superficial gas velocity for different sizes of particles. The predicted values and experimentally observed values of solid mass flux were compared and it was found to be in good agreement between them. The solid circulation increases with increase in superficial gas velocity and this may be explained by the fact that, the increase of upward drag forces resulted in increase of net rising particle velocity ($U - U_t$). The curves also show that the requirement of aeration flow was more for larger particles to initiate solids transport in the system. The aeration rates, which were needed to cause the minimum solids flow, were 0.08 m^3/h and 0.268 m^3/h for sand # I and sand # IV, respectively. At higher solid mass fluxes, the aeration flows were more than the minimum air flow required to initiate the solids flow.

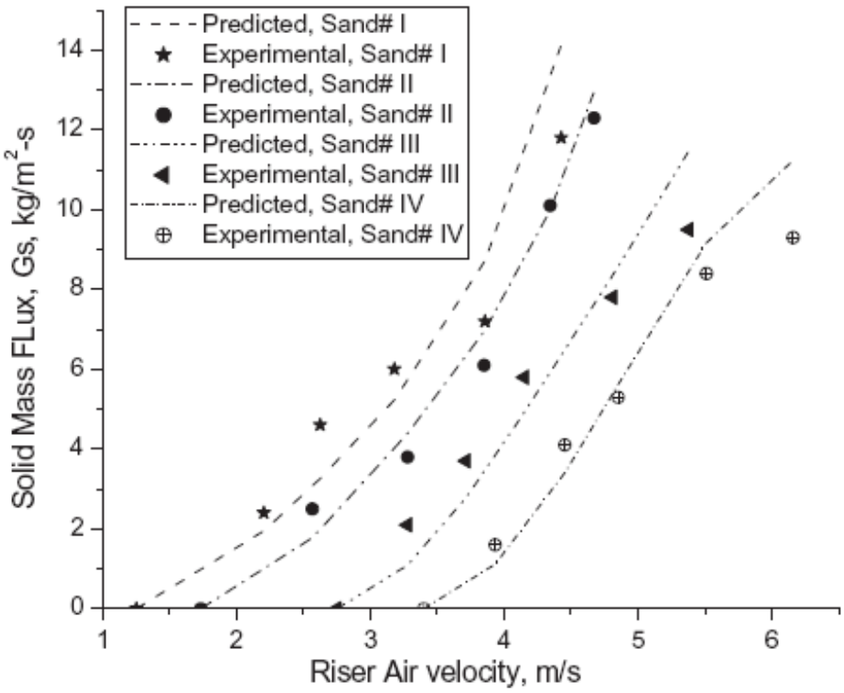

Fig. 9. Experimental and predicted mass fluxes (G_s) of samples at various riser air velocities.

3. Conclusion

The chapter gives a brief idea about the dual fluidized beds system, its experimental set up and the hydrodynamic model using L-valves in down comer and return leg. This model describes the essential features of the gas–solid flow structure. It was observed that the longitudinal voidage profiles in riser exhibit an exponential decay nature. Evaluation with experimental data shows sufficient accordance of the model regarding the pressure profile and the solids circulation. The solid circulation rate increases with increase in aeration flow and also with increase in superficial velocity. It was also discussed that, for lower size particles, the solid circulation is higher with the same superficial air flow. The L-valve aeration air requirement increases with increase in bed particle size and the pressure drop across L-valve is more for higher solid mass flux.

4. Acknowledgment

The authors thankfully convey heartfelt gratitude to Prof. Gautam Biswas, Director, CSIR - Central Mechanical Engineering Research Institute, Durgapur, India for his support during this research work..

5. References

Adanez, J. ; Gayan, P. ; Gracia-Labiano, F. & Diego, L. F. (1994). Axial voidage profiles in fast fluidized beds, *Powder Technology*, vol. 31, 259-268

Arena, U. ; Langeli, C.B. & Cammarota, A. (1998). L-Valve behavior with solids of different size and density, *Powder Technology* 98 231.

Bai, D. ; Issangya, A. S. ; Zhu, J. X. & Grace, J. R. (1997). Analysis of the overall pressure balance around a high-density circulating fluidized bed. *Industrial and Engineering Chemistry Research*, 36, 3898

Daous, M. A. & AI-Zahrani, A. A., (1998). Modeling solids and gas flow through an L-valve, *Powder Technology* vol 99, 86-89

Ergun, S. (1952) Fluid Flow Through Packed Columns. *Chem. Eng. Prog*., 48(2), 89

Geldart, D. & Jones, P. (1991). The behaviour of L-valves with Granular Powders, *Powder Technology*, 67 163-174

Gimbun, J. ; Chuah, T. G. ; Fakhru'l-Razi, A. & Choong, T. S. Y. (2005). The influence of temperature and inlet velocity on cyclone pressure drop: a CFD study, *Chem. Eng. and Processing* vol. 44, 7–12

Harris, B. J. & Davidson, J. F. (1994). Modeling options for circulating fluidized beds: A core/annulus deposition model, in A. A. Avidan (Ed), *Circulating fluidized bed technology IV*, 32-39, New York, AIChE.

Johnsson, F. ; Andersson, S. & Leckner, B. (1991). Expansion of a freely bubbling fluidized bed, *Powder Technology*, vol. 68, 117-123

Johnsson, F. & Leckner, B. (1995). Vertical distribution of solids in a CFB furnace, *13th Int. Conf. fluidized bed combustion*, 671-679, New York, ASME

Kaiser, S. ; Loffler, G. ; Bosch, K. & Hofbauer, H. (2003). Hydrodynamics of a dual fluidized-bed gasifier—Part II: simulation of solid circulation rate, pressure loop and stability, *Chemical Engineering Science*, vol.58, 4216 – 4223

Knowlton, T. M. (1977). Standpipe and return system in Circulating Fluidized Beds, 1st ed.; Grace, J. R., Avidan, A. A., Knowlton, T. M., Eds.; Blackie: London,; Chapter 7, p 240

Loffler, G. ; Kaiser S. ; Bosch, K. & Hofbauer, H. (2003). Hydrodynamics of a dual fluidized-bed gasifier—Part I: simulation of a riser with gas injection and diffuser, *Chemical Engineering Science*, vol.58, 4197 – 4213

Pugsley, T. S. & Berruti, F. (1996). A predictive hydrodynamic model for circulating fluidized bed risers, *Powder Technology*, vol. 89, 57-69

Pugsley, T. S. & Berruti, F. (1996).The circulating fluidized bed catalytic reactor; Reactor model validation and simulation of the oxidative coupling of methane, *Chem. Eng. Sci*., vol. 51, 2751-2756

Kim, W. K. ; Namkung, W. & Kim, S. D. (1999). Solid flow characteristics in loop-seal of a circulating fluidized bed, *Korean Journal of Chemical Engineering* 16 (1) 82–88.

Knowlton, T. M. & Hirsan, I. (1978). L-Valve Characterized for Solids Flow – Design Parameters Examined for Valve Use in Coal Gasification. *Hydrocarbon Processing*. Vol. 57, 149

Patience, G. S. ; Chaouki, J. & Grandjean, B. P. A. (1990). Solids Flow Metering from Pressure Drop Measurement in Circulating Fluidized Beds. *Powder Technology*. 61, 95

Schlichthaerle, P. & Werther, J. (1999). Axial pressure profiles and solids concentration distributions in the CFB bottom zone. *Chemical Engineering Science*, 54, 5485–5493

Tong, H. ; Hongzhong, L. ; Xuesong, L. & Qiayu, Z. (2003). Hydrodynamic modeling of the L-valve, *Powder Technology* vol 129, 8– 14

Wen, C. Y. & Chen, L. H. (1982). Fluidized bed freeboard phenomena: entrainment and elutriation, *AIChE Journal*, vol. 28, 117-128

Yang, W. (1978). A correlation for solid friction factor in vertical pneumatic conveying lines, *AIChE Journal*, vol. 24, 548-552

Zhang, J. Y. & Rudolph, V. (1991). Transitional Packed bed Flow in Standpipes, *Can. J. of Chem. Eng*., 69, 1242

Zenz, F. A. & Weil, N. A. (1958). A theoretical-emperical approach to mechanism of particle entrainment from fluidized beds, *AIChE Journal*, vol 4, 472-479

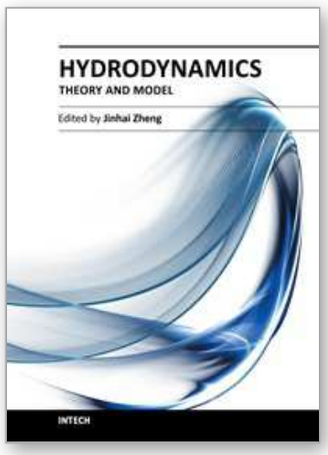

Hydrodynamics - Theory and Model

Edited by Dr. Jin - Hai Zheng

ISBN 978-953-51-0130-7
Hard cover, 306 pages
Publisher InTech
Published online 14, March, 2012
Published in print edition March, 2012

With the amazing advances of scientific research, Hydrodynamics - Theory and Application presents the engineering applications of hydrodynamics from many countries around the world. A wide range of topics are covered in this book, including the theoretical, experimental, and numerical investigations on various subjects related to hydrodynamic problems. The book consists of twelve chapters, each of which is edited separately and deals with a specific topic. The book is intended to be a useful reference to the readers who are working in this field.

How to reference

In order to correctly reference this scholarly work, feel free to copy and paste the following:

M.K. Karmakar and P.K. Chatterjee (2012). Hydrodynamics of Dual Fluidized Beds, Hydrodynamics - Theory and Model, Dr. Jin - Hai Zheng (Ed.), ISBN: 978-953-51-0130-7, InTech, Available from: http://www.intechopen.com/books/hydrodynamics-theory-and-model/hydrodynamics-of-dual-fluidized-beds

INTECH
open science | open minds

InTech Europe
University Campus STeP Ri
Slavka Krautzeka 83/A
51000 Rijeka, Croatia
Phone: +385 (51) 770 447
Fax: +385 (51) 686 166
www.intechopen.com

InTech China
Unit 405, Office Block, Hotel Equatorial Shanghai
No.65, Yan An Road (West), Shanghai, 200040, China
中国上海市延安西路65号上海国际贵都大饭店办公楼405单元
Phone: +86-21-62489820
Fax: +86-21-62489821

IntechOpen